# Aβ-PET Pattern Prediction via Graph Reconstruction-Aware Fusion (GRAF) of Functional and Structural Networks

Haoyue Yuan[1], Yuxiao Liu[1], Feihong Liu[1(✉)], Dinggang Shen[1,2,3(✉)]

[1] School of Biomedical Engineering & State Key Laboratory of Advanced Medical Materials and Devices, ShanghaiTech University, Shanghai 201210, China
sinceow@gmail.com, Dinggang.Shen@gmail.com
[2] Shanghai United Imaging Intelligence Co., Ltd., Shanghai 200030, China
[3] Shanghai Clinical Research and Trial Center, Shanghai 201210, China

**Abstract.** Alzheimer's disease (AD) is characterized by abnormal amyloid-β (Aβ) deposition, which causes neural damage and cognitive decline. Aβ positron emission tomography (PET) serves as the gold standard for preclinical diagnosis of AD. However, practical limitations, including high costs, radiation exposure, and constrained accessibility, have motivated recent studies to indirectly predict Aβ deposition patterns from MRI data. Unfortunately, existing methods have not fully leveraged the coupled pathological information from both functional and structural brain networks. To address this gap, we propose Graph Reconstruction-Aware Fusion (GRAF), a novel framework designed to predict regional Aβ-PET patterns by integrating functional and structural pathological information. GRAF employs a graph-masked autoencoder to learn integrated network topology embeddings by reconstructing masked edges from both functional and structural networks, effectively utilizing node and edge features. Subsequently, the well-trained encoders are fine-tuned to predict regional Aβ patterns. Extensive experimental results demonstrate that our proposed GRAF framework outperforms six state-of-the-art methods. Our code and representative case examples are publicly available at `https://github.com/ninicassiel/GRAF`.

**Keywords:** Alzheimer's disease · Amyloid-β PET · Self-supervised learning · Brain functional-structural network fusion.

## 1 Introduction

Alzheimer's disease (AD) is a prevalent and currently incurable neurodegenerative disorder characterized primarily by the abnormal accumulation of amyloid-β (Aβ), critically disrupting cognitive functions [11,13]. In the early phases of disease, excessive Aβ deposition triggers a cascade of pathological events, resulting functional and structural damage, making it a pivotal biomarker for diagnosis of preclinical AD [21]. Detecting these early pathological changes before clinical symptoms emerge offers a significant opportunity for timely intervention [13].

Clinically, Aβ positron emission tomography (PET) is the gold standard for *in-vivo* quantifying cerebral Aβ burden, providing vital insights into disease progression. However, despite its diagnostic value, the widespread use of Aβ-PET is hindered by high costs, radiation exposure, and limited accessibility, which are particularly pronounced challenges in resource-limited settings [12]. Therefore, there is an urgent need for alternative, cost-effective, and non-invasive methods to infer pathological progression, facilitating preclinical diagnosis and interventions for AD.

Recent advances in MRI techniques have enabled the modeling of complex brain neural systems as functional and structural networks, capturing dynamic blood oxygen level-dependent (BOLD) related cognitive activities and white matter connectivity, respectively [26]. Network attributes have increasingly been recognized as sensitive indicators of neural damage caused by Aβ deposition, underscoring their potential as biomarkers for preclinical AD diagnosis [26,28]. Accordingly, graph neural networks (GNNs) have been widely applied to extract sensitive features from both functional and structural networks for early diagnosis of AD [7,10]. Furthermore, GNN-based approaches have also demonstrated enhanced accuracy in diagnosing various other neurodegenerative disorders [1,27].

In addition to diagnostic applications, recent investigations have directly associated alterations in functional connectivity networks (FCNs) with cortical Aβ deposition [26]. These findings suggest that resting-state fMRI (rs-fMRI) signals could serve as effective correlates of Aβ burden as characterized by PET imaging. For example, Li et al. predicted regional standard uptake value ratios (SUVR) of cortical Aβ deposition from FCNs [5]. Liu et al. utilized a Large Language Model (LLM) to extract features from FCNs [12]. However, these studies have primarily relied on rs-fMRI alone and overlooked the integration of structural connectivity networks (SCNs) obtained from diffusion MRI (dMRI), despite evidence demonstrating that structural network topology and the loss of local structural connectivity contribute to AD diagnosis and the prediction of cortical Aβ deposition [4,7].

In this paper, to fully exploit the complementary functional and structural information from fMRI and dMRI data, we propose a graph reconstruction-aware fusion (GRAF) framework for integrating FCNs and SCNs in predicting regional Aβ-PET patterns. GRAF comprehensively characterizes Aβ-related functional and structural alterations, providing an accurate and robust prediction of Aβ-PET patterns and highlighting its potential for preclinical screening of AD. The main contributions of this paper are summarized as follows:

- We propose the GRAF framework based on a graph-masked autoencoder, which integrates node and edge features in FCNs and SCNs, to fully extract integrated embedding features by reconstructing masked edges.
- We introduce the Node-Edge Bidirectional Encoder specifically formulated to effectively utilize both node features and edge features from brain networks.
- We develop a cross-attention module specifically designed to leverage complementary information from both functional and structural networks.

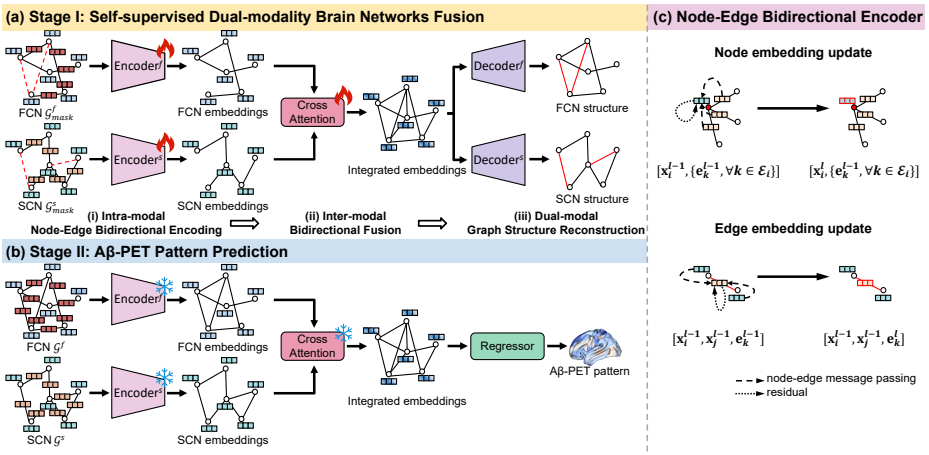


**Fig. 1.** Illustration of our proposed GRAF for Aβ-PET prediction, which consists of two stages. (a) Stage I, self-supervised dual-modality brain networks fusion; (b) Stage II, Aβ-PET pattern prediction; (c) The detailed structure of the node-edge bidirectional encoder.

## 2 Method

Our proposed GRAF consists of two stages, as shown in Fig. 1. In Stage I, we introduce a Self-supervised Dual-modality Brain Networks Fusion module, to integrate cross-modality information using a masked graph reconstruction strategy. In Stage II, we fine-tune the trained network components in Stage I and exploit the integrated embedding to predict the regional Aβ-PET SUVR patterns using the MLP regressor.

### 2.1 Dual-Modality Brain Networks

The brain network can be mathematically formulated as a graph $\mathbf{G} = (\mathcal{V}, \mathcal{E}, \mathbf{A})$, where $\mathcal{V}$ denotes $N_v$ nodes (regions of interest, ROIs), $\mathcal{E} \subseteq \mathcal{V} \times \mathcal{V}$ denotes $N_e$ edges, connecting pairs of ROIs, $\mathbf{A}$ denotes the adjacency matrix. Instead of treating edges as an element of $\mathbf{A}$, we propose to additionally employ them as edge features and introduce a specific module to integrate features across nodes and edges in FCNs and SCNs, respectively (see Fig.1 (c)).

FCNs are specifically denoted by $\mathbf{G}^f = (\mathcal{V}^f, \mathcal{E}^f, \mathbf{A}^f)$. In this work, $N_v^f = 100$ and node features $\mathbf{X}^f \in \mathbb{R}^{N_v^f \times 16}$ are derived from BOLD signals using a 1D-CNN to capture task-related temporal dynamics. The edges are defined by using Pearson's correlation coefficients, resulting in the adjacency matrix $\mathbf{A}^f$ and edge features $\mathbf{E}^f \in \mathbb{R}^{N_e^f \times 1}$. Meanwhile, SCNs are denoted by $\mathbf{G}^s = (\mathcal{V}^s, \mathcal{E}^s, \mathbf{A}^s)$, node features $\mathbf{X}^s \in \mathbb{R}^{N_v^s \times 3}$ are manually extracted from the adjacency matrix $\mathbf{A}^s$ based on topological attributes, including degree, betweenness, and closeness

centrality, using Brain Connectivity Toolbox [15]. Edge features $\mathbf{E}^s \in \mathbb{R}^{N_e^s \times 3}$ include the mean white matter microstructural attributes along the tract connecting a pair of nodes, *i.e.*, axial, mean, and radial diffusivity. Both functional and structural networks, $N_v^f = N_v^s$, are derived from the same Schaefer atlas with 100 ROIs [16].

### 2.2 Self-supervised Dual-modality Brain Networks Fusion

To guarantee feature representation and fusion across FCNs and SCNs, we first employ a self-supervised graph reconstruction framework exploiting both node and edge features of each brain network (as depicted in Fig.1 (a)). The encoders (as detailed in Fig. 1 (c)) first perform intra-modal node-edge bidirectional message passing to learn modality-specific embeddings. Then, a cross-attention module is introduced to integrate the FCNs and SCNs embeddings together thereby mutually refining both modality-specific and integrated embeddings. Finally, the decoders recover the masked edges from the integrated embeddings.

**Graph Masking** We leverage the edge masking strategy to train the encoders and decoders in GRAF [17,25]. Specifically, we create a masked subgraph through sampling edges from a Bernoulli distribution: $\mathcal{E}_{\text{mask}} \sim \text{Bernoulli}(p)$, where the masking ratio $p$ is set to 0.4 in this work. The masking operation $\mathcal{T}$ generates a masked graph $\mathcal{G}_{\text{mask}} = \mathcal{T}(\mathcal{G})$, keeping only a subset of the edges from the original FCNs or SCNs.

**Node-Edge Bidirectional Encoder** To fully integrate information from both gray matter (nodes) and white matter (edges), we propose a novel *Node-Edge Bidirectional Encoder* that models both node and edge attributes via a separate integration manner: (1) edge-to-node and (2) node-to-edge.

Given node features $\mathbf{X} = \{\mathbf{x}_1, \mathbf{x}_2, ..., \mathbf{x}_{N_v}\}$, $\mathbf{x}_i \in \mathbb{R}^{d_v^{l-1}}$, and edge features $\mathbf{E} = \{\mathbf{e}_1, \mathbf{e}_2, ..., \mathbf{e}_{N_e}\}$, $\mathbf{e}_i \in \mathbb{R}^{d_e^{l-1}}$, our proposed encoder applies an edge-to-node attention mechanism to update node embeddings. As illustrated in Fig. 1 (c), for edges $e_k \in \mathcal{E}_i$ connected to a node $v_i$, the attention coefficient is given by,

$$\alpha_{ik} = \frac{\exp\left(\sigma\left(\mathbf{a}_e^\top \left[\mathbf{W}_n \mathbf{x}_i \parallel \mathbf{W}_e \mathbf{e}_k\right]\right)\right)}{\sum_{j \in \mathcal{E}_i} \exp\left(\sigma\left(\mathbf{a}_e^\top \left[\mathbf{W}_n \mathbf{x}_i \parallel \mathbf{W}_e \mathbf{e}_j\right]\right)\right)}, \tag{1}$$

where $\mathbf{W}_n \in \mathbb{R}^{d_v^{l-1} \times d_v^l}$ and $\mathbf{W}_e \in \mathbb{R}^{d_e^{l-1} \times d_e^l}$ are learnable projection matrices, $\mathbf{a}_e$ is the attention vector, and $\sigma$ represents the activation function. The node features are updated by aggregating edge features using attention coefficients. The updated node features are then also combined with the previous layer's node features using a residual concatenation, thereby indirectly fusing node-to-node features:

$$\mathbf{x}_i^l = \sigma\left(\mathbf{W}_e \cdot \text{MEAN}\left(\{\alpha_{ik}\mathbf{e}_k, \forall k \in \mathcal{E}_i\}\right)\right) \parallel \mathbf{x}_i^{l-1}. \tag{2}$$

The node-to-edge feature fusion is performed simultaneously. Edge features are updated by aggregating the features of the two connecting nodes, also followed by residual feature concatenation. For edge $e_k$, which connects nodes $v_i$ and $v_j$, the update rule is:

$$\mathbf{e}_k^l = \text{MEAN}\left(\mathbf{x}_i^{l-1}, \mathbf{x}_j^{l-1}\right) \parallel \mathbf{e}_k^{l-1}. \tag{3}$$

**Bidirectional Cross-attention Mechanism** Having extracted the two graph embeddings from functional and structural encoders, GRAF further employs a cross-attention mechanism to integrate them. For integrating node embeddings $\mathbf{X}^f, \mathbf{X}^s \in \mathbb{R}^{N_v \times d}$, we establish two symmetric attention modules: (1) *Structure-Guided Functional Refinement* and (2) *Function-Guided Structural Refinement*. In *Structure-Guided Functional Refinement* module, SCN embeddings act as queries, while FCN embeddings provide keys and values, resulting in $\mathbf{Z}^{fs} = \text{softmax}\left(\frac{\mathbf{Q}^s \mathbf{K}^{f\top}}{\sqrt{d}}\right)\mathbf{V}^f$. By contrast, in *Function-Guided Structural Refinement* module, $\mathbf{Z}^{sf}$ obtained from FCN embeddings act as queries while SCN embeddings provide keys and values. This mutual refinement *not only* enables the SCN embeddings to impose anatomical constraints on the FCN embeddings *but also* lets the FCN embeddings introduce dynamic functional context into the SCN embeddings, resulting in well-integrated embeddings:

$$\mathbf{Z} = [\mathbf{Z}^{fs} \parallel \mathbf{Z}^{sf}] \in \mathbb{R}^{N_v \times 2d}. \tag{4}$$

**Decoder** The graph reconstruction decoder $h_\omega$ predicts the existence of masked edges through,

$$h_\omega(\mathbf{z}_i, \mathbf{z}_j) = \text{Sigmoid}(\text{MLP}(\mathbf{z}_i \circ \mathbf{z}_j)), \tag{5}$$

where the element-wise product $\circ$ captures correlations among node embeddings $(\mathbf{z}_i, \mathbf{z}_j)$, and MLPs are incorporated to capture the nonlinearity in reconstructing FCNs and SCNs respectively from the same integrated embeddings, with the sigmoid normalization outputting probabilistic predictions $\in [0, 1]$.

**Learning objective** In stage I, GRAF targets to extract integrated embeddings to reconstruct both FCNs and SCNs. To achieve this, it employs binary cross-entropy to measure the model capacity in recovering the masked edges:

$$\mathcal{L} = -\left(\frac{1}{|\mathcal{E}^+|}\sum_{(i,j)\in\mathcal{E}^+} \log h_\omega(\mathbf{z}_i, \mathbf{z}_j) + \frac{1}{|\mathcal{E}^-|}\sum_{(i',j')\in\mathcal{E}^-} \log(1 - h_\omega(\mathbf{z}_{i'}, \mathbf{z}_{j'}))\right), \tag{6}$$

where $\mathcal{E}^+$ denotes the edges in $\mathcal{G}_{mask}$ that have been masked out, $\mathcal{E}^-$ denotes uniformly sampled negative edges (non-existent connections). $\mathcal{E}^+$ and $\mathcal{E}^-$ ensure a balanced objective, which guarantees accurate reconstruction of masked edges without introducing false-positive connections.

### 2.3 Aβ-PET Pattern Prediction

As depicted in Fig. 1 (b), after pre-training, GRAF utilizes the graph fusion architecture to process the complete FCNs $\mathcal{G}^f$ and SCNs $\mathcal{G}^s$. The integrated embeddings $\mathbf{Z}$ may not reveal the pathological information of AD during pre-training. To adapt the model for this downstream task, we further fine-tune the encoders and then train a Regressor (lightweight MLP) to map the integrated embeddings to regional Aβ-PET SUVRs. Mean squared error (MSE) between predicted and observed SUVRs across ROIs is employed to govern model fine-tuning.

## 3 Experiments and Results

### 3.1 Datasets and Preprocessing

We validate our framework on the in-house Huashan [2] dataset (524 subjects) with paired fMRI, dMRI, and PET data (435 subjects, with 194 Aβ positive, 285 Aβ negative and 45 unlabeled cases). All MRI data were acquired on a 3.0 T Siemens Prisma scanner. The Schaefer atlas (100 ROIs) [16] is co-registered to each individual space using the T1-weighted MRI brain template. The rs-fMRI data is processed using ANTs [19] and DPARSF [22]. The dMRI data is processed using FSL [3], ANTs [19], and MRtrix3 [18], with SCNs construction using SIFT2-weighted streamline counts. PET data underwent partial volume correction using the PET Unified Pipeline [14], where SUVRs are calculated by normalizing the target region SUV to the reference cerebellar values. Regional SUVRs are averaged within each ROI defined by the same Schaefer atlas.

### 3.2 Experimental Settings and Evaluation Metrics

During training the encoders, we employ the Adam optimizer with a learning rate of $5 \times 10^{-4}$ for $2,000$ epochs. To fully extract the topological attributes, the graph masking strategy is updated every 100 epochs (batch size = 32, mask ratio = 0.4). In the Aβ-PET pattern prediction stage of GRAF and all SOTA competing methods, we reduce the learning rate to $5 \times 10^{-5}$, using the Adam optimizer with weight decay set to $10^{-4}$, for a maximum of 500 epochs (batch size = 32). Comprehensive hyperparameter tuning preceded these settings, including optimizer selection (Adam vs. SGD), learning rates ($10^{-3}$ to $10^{-5}$; 10 equidistant trials), weight decay ($10^{-4}$ to $10^{-6}$; 10 equidistant trials), and the number of layers per block.

We compare our proposed method with six SOTA methods, such as the single modality GCN [24], GAT [20], and BrainGNN [6] using simple concatenation fusion strategy, as well as multimodal graph fusion methods, SCP-GCN [8], M-GNN [9], and Cross-GNN [23], where single-modality models specifically benchmark our dual-graph fusion approach while multimodal methods represented contemporary comparators. All methods employ the same Aβ-PET pattern regression module as GRAF.

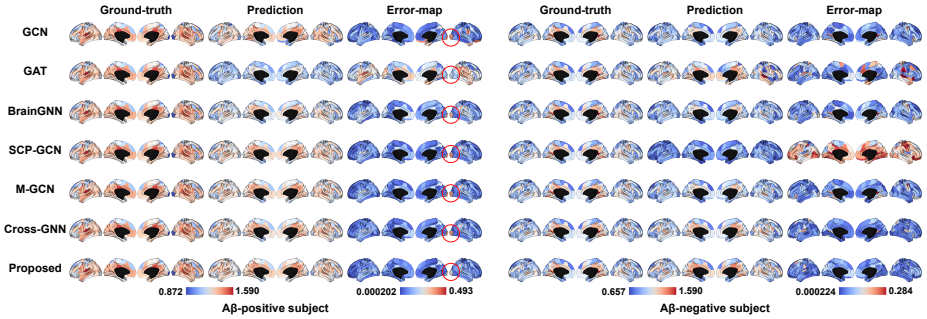


**Fig. 2.** Qualitative comparison results of regional Aβ-PET pattern prediction. The ground-truth, prediction, and error maps are shown for Aβ-positive and Aβ-negative subjects, respectively. The mean MAE values for these error maps of the Aβ positive subject are: 0.1210 (GCN), 0.2232 (GAT), 0.1219 (BrainGNN), 0.1156 (SCP-GCN), 0.1167 (M-GCN), 0.1190 (Cross-GCN), and **0.0816 (Proposed)**, respectively. Similar metrics for the Aβ negative subject are 0.0907 (GCN), 0.1040 (GAT), 0.0935 (BrainGNN), 0.1832 (SCP-GCN), 0.0689 (M-GCN), 0.0797 (Cross-GCN), and **0.0492 (Proposed)**.

All models are evaluated via 5-fold cross-validation. For evaluation, graph reconstruction was assessed by accuracy (ACC), sensitivity (SEN), specificity (SPE), and the area under the receiver operating characteristic curve (AUC), while the quality of generated Aβ-PET patterns is quantified through MSE, mean absolute error (MAE) and mean absolute percentage error (MAPE) against the real patterns.

### 3.3 Qualitative and Quantitative Results

**SOTA Comparisons** During pre-training, GRAF recovers edges achieving AUC as high as 0.88, and SEN, SPE, ACC as high as 0.78 for both FCNs and SCNs. We further fine-tune these encoders to predict the regional Aβ-PET patterns. Table 1 presents the Aβ-PET pattern prediction results, with

**Table 1.** Quantitative comparison results (mean ± standard deviation) of regional Aβ-PET pattern prediction.

| Method | | MSE ↓ | MAE ↓ | MAPE ↓ |
|---|---|---|---|---|
| Concat fusion | GCN | 0.0441 ± 0.0412 | 0.1635 ± 0.0791 | 0.1356 ± 0.0655 |
| | GAT | 0.0449 ± 0.0544 | 0.1638 ± 0.0997 | 0.1351 ± 0.0810 |
| | BrainGNN | 0.0455 ± 0.0582 | 0.1614 ± 0.1009 | 0.1237 ± 0.0604 |
| Intrinsic fusion | SCP-GCN | 0.0571 ± 0.0602 | 0.1919 ± 0.1019 | 0.1479 ± 0.0625 |
| | M-GCN | 0.0442 ± 0.0643 | 0.1581 ± 0.1023 | 0.1222 ± 0.0653 |
| | Cross-GNN | 0.0398 ± 0.0517 | 0.1502 ± 0.0941 | 0.1154 ± 0.0566 |
| | Proposed | **0.0211 ± 0.0155** | **0.1156 ± 0.0464** | **0.0960 ± 0.0367** |

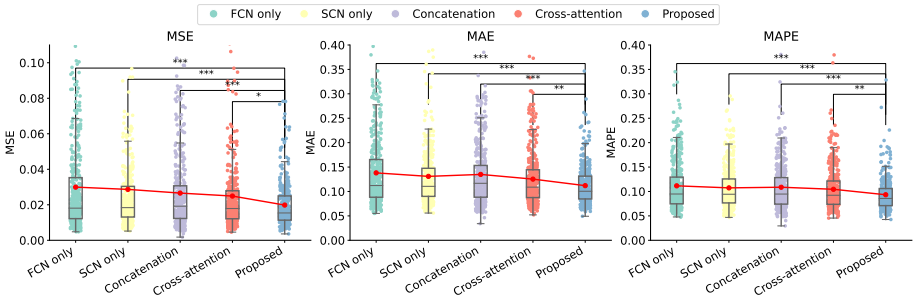


**Fig. 3.** Ablation study regarding each key component of our GRAF. $*$ denotes significant improvement of GRAF over other ablation models, as determined by Mann-Whitney U Test ($* : p < 0.05; ** : p < 0.01; *** : p < 0.001$). The red point stands for the mean value.

all ROI results averaged across the testing dataset in 5-fold cross-validation. Those graph-based methods with a simple fusion module, such as GCN, GAT, and BrainGNN, demonstrate close performance. However, M-GCN, Cross-GNN, and GRAF, with a specifically designed fusion module, generally exhibit superior representational capacity. In contrast, SCP-GCN demonstrates inferiority, which probably stems from its focus on preserving population-level features, which might overlook features at the individual level. Our proposed GRAF outperforms all others, achieving significantly lower errors (with $p < 0.05$), showing a 23.1% relative improvement in MAE over the second-best method, Cross-GNN. As shown in Fig. 2, we qualitatively demonstrate the ground-truth and predicted Aβ-PET patterns for carefully selected representative Aβ-negative and Aβ-positive subjects, who were matched for age and Mini-Mental State Examination scores. We can see that our proposed GRAF captures the ground-truth spatial patterns more accurately, especially in the occipital areas (highlighted by red circles), where competitive methods tend to falsely overestimate Aβ deposition, which is evidenced by higher errors and reflected in the wider color-bar range.

**Ablation Study** To assess the efficacy of our proposed modules in GRAF, we conduct a comprehensive ablation study with various configurations: (1) FCNs only; (2) SCNs only; (3) Concatenation (fusion via simply concatenating FCN and SCN features); and (4) Cross-attention (fusion via cross-attention) but in an end-to-end training manner. Fig. 3 depicts the distribution of errors across the testing dataset. We can find that the Cross-attention configuration demonstrates the most improvements over other configurations. Notably, our proposed GRAF, which employs a two-stage training strategy, outperforms the end-to-end training strategy, *i.e.*, configuration (4), even it has the same dual-modality fusion strategy.

## 4 Conclusion

We introduce GRAF, a graph reconstruction-aware fusion framework to predict the regional Aβ-PET patterns using both functional and structural networks. To the best of our knowledge, GRAF is the first attempt to exploit both functional and structural networks capturing neural damage that is mostly correlated with Aβ deposition. The two-stage training paradigm effectively separates feature representation from specific downstream tasks, which alleviates the issue of limited MRI-PET paired data. Furthermore, our node-edge bidirectional information transfer encoder integrates both node (gray matter) and edge (white matter) attributes. Both quantitative and qualitative experimental results demonstrate the high predictive accuracy achieved by GRAF, demonstrating its potential in characterizing pathological progression in early AD phases. Future work will address current limitations, including demographic variability, disease stage heterogeneity, and data imbalance, through multi-stage pretraining and multitask learning to enhance GRAF's generalizability and predictive performance.

**Acknowledgments.** This work was supported in part by National Natural Science Foundation of China (grant numbers 62131015, 62250710165, U23A20295, 62203355), the STI 2030-Major Projects (No. 2022ZD0209000), Shanghai Municipal Central Guided Local Science and Technology Development Fund (grant number YDZX20233100001001), Science and Technology Commission of Shanghai Municipality (STCSM) (grant number 21010502600), The Key R&D Program of Guangdong Province, China (grant numbers 2023B0303040001, 2021B0101420006) and HPC Platform of ShanghaiTech University.

**Disclosure of Interests.** The authors have no competing interests to declare that are relevant to the content of this article.

## References

1. Cui, H., Dai, W., Zhu, Y., Li, X., He, L., Yang, C.: Interpretable graph neural networks for connectome-based brain disorder analysis. In: International Conference on Medical Image Computing and Computer-Assisted Intervention. pp. 375–385. Springer (2022)
2. Ding, D., Zhao, Q., Guo, Q., Liang, X., Luo, J., Yu, L., Zheng, L., Hong, Z.: Progression and predictors of mild cognitive impairment in chinese elderly: A prospective follow-up in the shanghai aging study. Alzheimer's Dementia: Diagnosis, Assessment Disease Monitoring **4**, 28–36 (2016)
3. Jenkinson, M., Beckmann, C.F., Behrens, T.E.J., Woolrich, M.W., Smith, S.M.: FSL. NeuroImage **62**(2), 782–790 (2012)
4. Kantarci, K., Schwarz, C.G., Reid, R.I., Przybelski, S.A., Lesnick, T.G., Zuk, S.M., Senjem, M.L., Gunter, J.L., Lowe, V., Machulda, M.M., et al.: White matter integrity determined with diffusion tensor imaging in older adults without dementia: influence of amyloid load and neurodegeneration. JAMA neurology **71**(12), 1547–1554 (2014)

5. Li, C., Liu, M., Xia, J., Mei, L., Yang, Q., Shi, F., Zhang, H., Shen, D.: Predicting brain amyloid-$\beta$ PET grades with Graph Convolutional Networks based on functional MRI and multi-level functional connectivity. Journal of Alzheimer's Disease **86**(4), 1679–1693 (2022)
6. Li, X., Zhou, Y., Dvornek, N., Zhang, M., Gao, S., Zhuang, J., Scheinost, D., Staib, L.H., Ventola, P., Duncan, J.S.: BrainGNN: Interpretable brain Graph Neural Network for fMRI analysis. Medical Image Analysis **74**, 102233 (2021)
7. Liu, F., Pan, Y., Yang, J., Xie, F., He, X., Zhang, H., Shi, F., Feng, J., Guo, Q., Shen, D.: Identifying alzheimer's disease-induced topology alterations in structural networks using convolutional neural networks. In: International Workshop on Machine Learning in Medical Imaging. pp. 33–42. Springer (2023)
8. Liu, J., Ma, G., Jiang, F., Lu, C.T., Philip, S.Y., Ragin, A.B.: Community-preserving graph convolutions for structural and functional joint embedding of brain networks. In: 2019 IEEE International Conference on Big Data (Big Data). pp. 1163–1168. IEEE (2019)
9. Liu, J., Ma, G., Jiang, F., Lu, C.T., Philip, S.Y., Ragin, A.B.: M-GCN: A multimodal graph convolutional network to integrate functional and structural connectomics data to predict multidimensional phenotypic characterizations. In: Medical Imaging with Deep Learning. pp. 119–130. PMLR (2021)
10. Liu, M., Zhang, H., Shi, F., Shen, D.: Hierarchical graph convolutional network built by multiscale atlases for brain disorder diagnosis using functional connectivity. IEEE Transactions on Neural Networks and Learning Systems (2023)
11. Liu, M., Zhang, D., Adeli, E., Shen, D.: Inherent structure-based multiview learning with multitemplate feature representation for alzheimer's disease diagnosis. IEEE Transactions on Biomedical Engineering **63**(7), 1473–1482 (2015)
12. Liu, Y., Liu, M., Zhang, Y., Guan, Y., Guo, Q., Xie, F., Shen, D.: Amyloid-$\beta$ deposition prediction with large language model driven and task oriented learning of brain functional networks. IEEE Transactions on Medical Imaging (2025)
13. Long, J.M., Holtzman, D.M.: Alzheimer disease: an update on pathobiology and treatment strategies. Cell **179**(2), 312–339 (2019)
14. Moulder, K.L., Snider, B.J., Mills, S.L., Buckles, V.D., Santacruz, A.M., Bateman, R.J., Morris, J.C.: Dominantly inherited alzheimer network: facilitating research and clinical trials. Alzheimer's research & therapy **5**, 1–7 (2013)
15. Rubinov, M., Sporns, O.: Complex network measures of brain connectivity: uses and interpretations. NeuroImage **52**(3), 1059–1069 (2010)
16. Schaefer, A., Kong, R., Gordon, E.M., Laumann, T.O., Zuo, X.N., Holmes, A.J., Eickhoff, S.B., Yeo, B.T.T.: Local-global parcellation of the human cerebral cortex from intrinsic functional connectivity MRI. Cerebral cortex **28**(9), 3095–3114 (2018)
17. Thakoor, S., Tallec, C., Azar, M.G., Munos, R., Veličković, P., Valko, M.: Bootstrapped representation learning on graphs. In: ICLR 2021 workshop on geometrical and topological representation learning (2021)
18. Tournier, J.D., Smith, R., Raffelt, D., Tabbara, R., Dhollander, T., Pietsch, M., Christiaens, D., Jeurissen, B., Yeh, C.H., Connelly, A.: MRtrix3: A fast, flexible and open software framework for medical image processing and visualisation. NeuroImage **202**, 116137 (2019)
19. Tustison, N.J., Avants, B.B., Cook, P.A., Zheng, Y., Egan, A., Yushkevich, P.A., Gee, J.C.: N4ITK: improved N3 bias correction. IEEE Transactions on medical imaging **29**(6), 1310–1320 (2010)

20. Veličković, P., Cucurull, G., Casanova, A., Romero, A., Liò, P., Bengio, Y.: Graph Attention Networks. In: International Conference on Learning Representations (ICLR) (2018)
21. Xing, X., Li, Q., Yuan, M., Wei, H., Xue, Z., Wang, T., Shi, F., Shen, D.: DS-GCNs: Connectome classification using dynamic spectral graph convolution networks with assistant task training. Cerebral Cortex **31**(2), 1259–1269 (2021)
22. Yan, C., Zang, Y.: DPARSF: a matlab toolbox for" pipeline" data analysis of resting-state fMRI. Frontiers in systems neuroscience **4**, 1377 (2010)
23. Yang, Y., Ye, C., Guo, X., Wu, T., Xiang, Y., Ma, T.: Mapping multi-modal brain connectome for brain disorder diagnosis via cross-modal mutual learning. IEEE Transactions on Medical Imaging **43**(1), 108–121 (2023)
24. Yao, L., Mao, C., Luo, Y.: Graph convolutional networks for text classification. In: Proceedings of the AAAI conference on artificial intelligence. vol. 33, pp. 7370–7377 (2019)
25. You, Y., Chen, T., Sui, Y., Chen, T., Wang, Z., Shen, Y.: Graph contrastive learning with augmentations. Advances in neural information processing systems **33**, 5812–5823 (2020)
26. Yu, M., Sporns, O., Saykin, A.J.: The human connectome in alzheimer disease—relationship to biomarkers and genetics. Nature Reviews Neurology **17**(9), 545–563 (2021)
27. Zhang, Y., Huang, H.: New graph-blind convolutional network for brain connectome data analysis. In: International conference on information processing in medical imaging. pp. 669–681. Springer (2019)
28. Zhang, Y., Sun, K., Liu, Y., Xie, F., Guo, Q., Shen, D.: A modality-flexible framework for alzheimer's disease diagnosis following clinical routine. IEEE Journal of Biomedical and Health Informatics (2024)